Astron. Astrophys. 343, 287–296 (1999)

ASTRONOMY AND ASTROPHYSICS

Radio evidence on shock wave formation in the solar corona

A. Klassen[1], **H. Aurass**[1], **K.-L. Klein**[2], **A. Hofmann**[1], **and G. Mann**[1]

[1] Astrophysikalisches Institut Potsdam, An der Sternwarte 16, D-14482 Potsdam, Germany
[2] Observatoire de Paris, Section de Meudon, DASOP and URA 2080, F-92195 Meudon Principal Cedex, France

Received 27 August 1998 / Accepted 2 December 1998

Abstract. In order to investigate the formation of radio emitting shock waves above flaring active regions, we combine spectral and imaging observations of type II radio events with X-ray imaging and full-Sun observations and, in one case, with the extrapolated magnetic field configuration in the corona. We confirm and extend earlier findings that type II bursts are emitted above active region loops seen in soft X-ray images. Sources at successively lower frequencies are non-radially displaced from the axis of the active region loops. Two new radio features identified in high resolution spectrograms establish a possible link between the type II emission and the preceding activity in the underlying corona:

1. Groups of fast drift bursts or pulsations with a restricted bandwidth are observed in coronal loops from the impulsive flare phase until the onset of the type II emission. These groups or their high frequency cut-off are found in the spectral range around the backward extrapolated type II lanes. Envelope features of the group (starting frequency and/or cut-off frequency) drift gradually to lower frequencies, at a normalized drift rate similar to the following type II lanes. The sources are located between the sites of Hα emission and of the type II emission. We refer to this burst group and its envelope features as a *type II precursor*.
2. Immediately before the type II emission a short ($\leq$ 1 min duration) series of narrow-band bursts occurs at frequencies between the split bands of the type II lanes. As a whole, the burst sequence has an inverted U–shaped spectral envelope. We therefore call it an *arc*. It has fundamental-harmonic structure as the subsequent type II burst, but no band split. The source is located near or above the summits of the coronal loops where the *precursor* emission occurred before, and close to the site where the type II emission starts. The *arc* feature occurs especially prior to high frequency type II bursts, i.e. type II shocks formed at comparatively low coronal height.

It is concluded that the type II burst is related to a plasma jet or a blast wave that originates in closed magnetic structures in the active region, and is first recognized during the early impulsive phase (between the onset and main maximum of the hard X-ray emission). This disturbance becomes or launches a shock wave when it attains the summit of these structures. The shock is refracted into overlying field regions, where it becomes visible through the type II emission.

Key words: shock waves – Sun: corona – Sun: flares – Sun: magnetic fields – Sun: radio radiation

Send offprint requests to: A. Klassen (aklassen@aip.de)

1. Introduction

While solar type II bursts are generally ascribed to large-scale coronal shock waves, the origin of these disturbances has still not been identified. In a recent attempt to trace the type II radio signature back to lower atmospheric layers, Vršnak et al. (1995, with references to earlier work) found that the peak time of the microwave burst is a plausible estimate of the ignition time of the disturbance. On the other hand, Aurass, Magun and Mann (1994) identified radio spectral fine structures that suggest the disturbance is launched at greater heights. Both findings add evidence to the idea that the type II shock wave is related with flare energy release, as opposed to the bow shock of a coronal mass ejection (cf. Gopalswamy and Kundu (1992), Gopalswamy et al. (1998); Aurass (1997 for a recent review)). Gopalswamy et al. (1997) presented a case study giving evidence that a complex radio burst comprising a type II shock is related with the ejection of material imaged by *Yohkoh* Soft X-ray Telescope, and suggested that events which show no such piston should not be accompanied by type II emission either. Different aspects of type II burst observations are summarized in Nelson & Melrose (1985), Bougeret (1985), Hildner et al. (1986), Aurass (1992, 1997) and Mann (1995). Recent theoretical work on electron acceleration in coronal shocks was published by Mann et al. (1995) and Mann & Classen (1995)

We search for radio signatures between the onset of the impulsive flare phase, revealed by the rise of the hard X-ray (HXR) emission, and the onset of the type II emission. The use of sensitive digital radio spectrography and radio imaging with high time resolution, combined with imaging and full-Sun observations in X-rays, improve our ability to discover weak radio features and to infer their link with coronal structures. The present paper uses observations of the Tremsdorf Spectro-

graph of the Potsdam Astrophysical Institute, the Nançay Radioheliograph, the *Yohkoh* SXT, and full-Sun recordings of the hard X-ray (BATSE aboard the *Compton Gamma-Ray Observatory* (CGRO)) and soft X-ray (GOES satellite) fluxes. The radio instruments and the data selection are outlined in Sect. 2.1. The observations of five individual events are presented in Sect. 2.2. We corroborate and extend former findings on the location of the type II sources with respect to coronal structures, and detect new features relevant to the propagation of the coronal disturbance which eventually gives rise to the shock wave. These results are summarized in Sect. 2.3, and discussed in Sect. 3.

2. The observations

2.1. Instruments and data selection

The radio observations were carried out with the spectrograph of the Tremsdorf Solar Radio Observatory of the Astrophysical Institute (AI) Potsdam and the Nançay Radioheliograph (NRH). The AI Potsdam instrument consists of swept-frequency spectrographs in the ranges 40–90, 100–170, 200–400 and 400–800 MHz, with a sweep rate of 10 s^{-1} (Mann et al. 1992). The dynamic spectrograms are digitally recorded. The NRH provided ten one-dimensional scans of the corona per second at five frequencies in the range 150–450 MHz, with both its east-west and north-south branches (The Radioheliograph Group 1989). *Yohkoh* SXT images (Tsuneta et al. 1991) and the necessary software were provided by the *Yohkoh* community. BATSE hard X-ray and GOES soft X-ray data were provided by the *Solar Data Analysis Center* (SDAC) at Goddard Space Flight Center.

For the present analysis we selected five events in the years 1993 and 1994 which were observed by all mentioned data sources. Thereby some selection effect results from the demanded coverage of very narrow band spectral features by the given discrete observing frequencies of the NRH. This leads to a preference for type II bursts with starting frequency above 164 MHz (the lowest NRH frequency).

2.2. Description of individual events

2.2.1. 13 July 1994

The event of Fig. 1 contains a type II burst with a dominant harmonic lane, band split, and herringbone drift bursts emanating from the backbone. The type II lane starts at 11:46:15 UT. It is preceded by three groups of spectrally distinct features (cf. spectra in Fig. 1a, centroid positions of the radio sources superposed on a *Yohkoh* SXT image in Fig. 1c):

1. An initial group of fast drift bursts (type III, J, U) covers the band from 300 MHz down to the low frequency limit of the spectrograph at 40 MHz. The bursts cease around 11:42 UT at frequencies below 170 MHz. The sources of type III bursts and of the ascending branches of J and U-bursts at 164 MHz (big crosses, Fig. 1c) are located north-west of the site of Hα emission (white diamond). The descending branches of U bursts (small crosses) are all north-east of the Hα flare site. The 164 MHz sources outline closed magnetic structures in east-west direction. They are only seen as diffuse features in the *Yohkoh* SXT image, but the north-south orientation of the inversion line of the large-scale photospheric magnetic field (cf. Stanford magnetograms on 11 and 14 July, SGD 601-I) corroborates this interpretation. Some faint 237 MHz sources are close to the top of this loop structure.
2. A less densely packed group of fast drift bursts with restricted bandwidth ($\leq$ 30% of the centre frequency), having predominantly negative drift rates appears near 11:42 UT above the frequency gap 170–200 MHz (see the enlargement in Fig. 2). The burst sequence extends abruptly to lower frequencies (110 MHz) after 11:43:20 UT. The centre frequency of this group lies near the backward extrapolated straight line through the type II lane after $\sim$11:47 UT. The high frequency cut-off of the group gradually drifts towards lower frequencies at a normalized drift rate $-D_f/f$ (where D_f =df/dt, f is the frequency) between $2 \cdots 4{\cdot}10^{-3}$ s^{-1}, comparable to the rate of the subsequent type II lane ($-D_f/f = 2.6 \cdot 10^{-3}\ s^{-1}$, Table 1). The bursts occur in a similar structure as the fast drift bursts before 11:42 UT. Because of the frequency range and the similar relative drift rate to the type II lane we refer to the burst group as *type II precursor* in the following. We note that the high frequency cut-off of the initial burst group is also near the backward extrapolated type II lane.
3. The type II burst is preceded (between 11:45:20 and 11:46:15 UT, see also Fig. 9) by a dense sequence of fast drift bursts. Its spectral envelope has the shape of an inverted U or an arc, with a similar bandwidth as the subsequent type II lane. We call this feature an *arc*. Radioheliographic data at 164 MHz are available only for the high frequency part of a few individual bursts of the *arc*. The source is near the summit of the loop system hosting the preceding bursts (Fig. 1c), and close to the site of the subsequent type II emission. The type II burst itself starts together with a faint type III burst that extends down to 100 MHz.

No hard X-ray data are available for this event. Using the derivative of the soft X-ray flux time history as a proxy (stippled line in Fig. 1b, cf. Dennis & Zarro 1993, and references therein), we find that both the initial fast drift burst group and the *type II precursor* are accompanied by energy deposition in the low atmosphere as outlined by the positive derivative of the GOES 1–8 Å flux. Consequently, we consider these radio features as elements of the impulsive flare phase. The *arc* occurs in the decay phase of the soft X-ray burst.

2.2.2. 27 September 1993

The event (Fig. 3) displays three harmonically (1 : 2 : 3) related type II burst lanes. This phenomenon was discussed by Aurass, Klein and Mann (1994) and Zlotnik et al. (1998). We briefly describe the global evolution and source positions with respect to the features identified in the 13 July 1994 event:

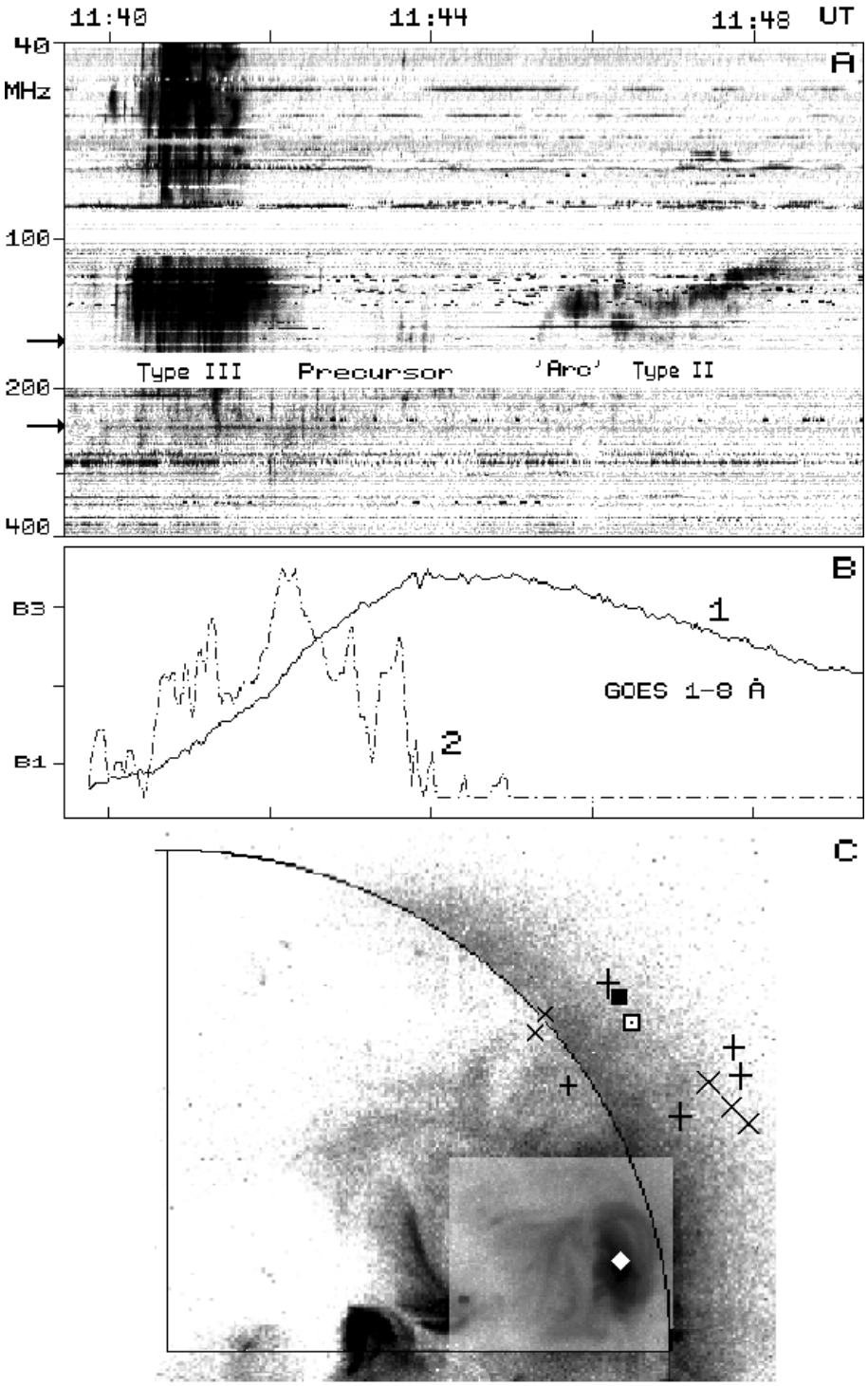

Fig. 1a–c. Event on 13 July 1994. **a** the 40–400 MHz dynamic spectrum after background subtraction. White time-parallel stripes are observational gaps. Arrows point at given NRH frequencies, **b** GOES soft X-ray flux 1–8 Å (1) and its derivative (2) (units as in SGD- Solar Geophysical Data, B1 = $10^{-4}\ erg\ (cm^2\ s)^{-1}$, **c** burst positions superposed upon the *Yohkoh* SXT image (12:33 UT): $\diamond$ – Hα flare, $\times$ ($\times$) – the ascending (descending) branch of the group of type III, J and U bursts at 164 MHz, $+$ (+) – the ascending (descending) branch of *type II precursor* at 164 and 236 MHz, $\boxdot$ – 'arc', $\blacksquare$ – type II burst. North is toward the top; west is toward the right.

1. The initial impulsive phase emission (12:07–12:09 UT) comprises bursts of types J and U whose cut-offs at low and high (decimetric) frequencies converge in the course of time to a narrow range around 280 MHz. The low frequency cut-off of the burst group is in the frequency range of the fundamental type II burst. Fast drift bursts at longer metric wavelengths (below 100 MHz) are missing. Simultaneously, radio emission starts at a frequency of about 2–3 GHz and drifts towards lower frequencies at a rate $2.5 \cdot 10^{-2}\ s^{-1}$. On this drifting continuum emission fast reverse drifting bursts in the range 2–4 GHz are superimposed (Fig. 3b, see also Karlický and Jiřička 1996).
2. Before the end of the initial impulsive metric group decimetric pulsations start near its high frequency cut–off (400–800 MHz, 12:08:15-12:09:15 UT). When the pulsations start, the emission above 1 GHz shifts to lower fre-

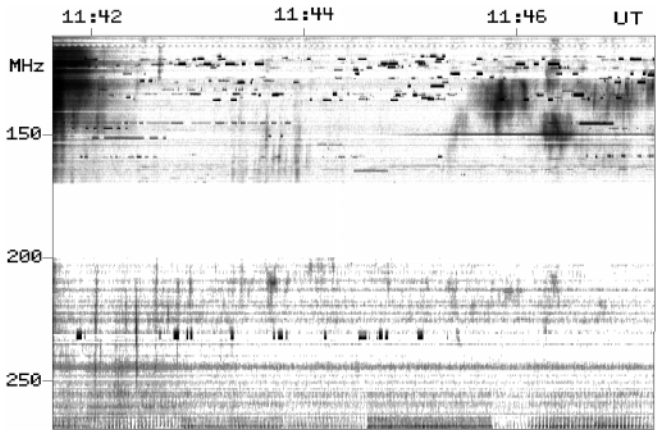

Fig. 2. Event on 13 July 1994. The 110–270 MHz dynamic spectrum of the *type II precursor.*

quencies. The separation between the J/U bursts and the pulsations gradually drifts toward lower frequencies. The group of pulsations, the dividing line with the J/U bursts, and the drifting leading edge of the underlying continuum emission near 800 MHz lie in the backward extrapolation of the second harmonic type II lane. Because of their spectral properties we identify these features as signatures of a *type II precursor*.

3. The type II lanes are preceded by an *arc* (12:10:00–12:10:40 UT). Although the *arc* is only partly visible in the fundamental mode due to the gap of spectral observations (170–200 MHz), it is seen to have the same fundamental–second harmonic–third harmonic pattern as the type II burst. The observations of the harmonic band show, however, that the *arc* does not display the band split as the type II lane. The *arc* is accompanied by microwave emission and by minor hard X-ray peaks.

Hard X-ray emission accompanies all three groups of radio bursts. The highest count rates are observed during the initial J/U bursts and the pulsations. The count rates become weaker as the radio emission shifts to lower frequencies.

Fig. 4 shows the radio source positions overlaid on the difference between the *Yohkoh* SXT post-flare (12:37:17 UT) and pre-flare (12:00:29 UT) images. The basic structure in the difference image is a dark rim around a white (roughly speaking unchanged) region above the limb. The outer border of the rim is outside the field of view. When on the disk, the active region consists of bundles of east-west oriented X-ray loops. It is hence likely that the features in the difference image are mostly southward-tilted loops seen edge-on. The radio sources between 435 and 237 MHz during the impulsive phase, including type J and III bursts and pulsations, project onto these regions where the most pronounced enhancements of density or temperature occur. The burst sources brighten pairwise. The brighter component is denoted by black crosses, the weaker one by white crosses. The 164 MHz emission occurs above and south of a bright jet-like feature at the southern border of the perturbed configuration. The *arc* sources in the corresponding harmonics occur at different positions (not shown in Fig. 4). Second and third harmonic type II sources (filled squares) are cospatial and non-radially aligned above the inferred loop system. They start with a distinct separation (about 80000–100000 km) from the harmonic *arc* source, but above the *precursor* burst sources. The arrow interconnecting filled squares describes the outward motion of the type II exciter as traced by the brightening of harmonic mode sources at successively lower frequencies (410, 327, 237 MHz).

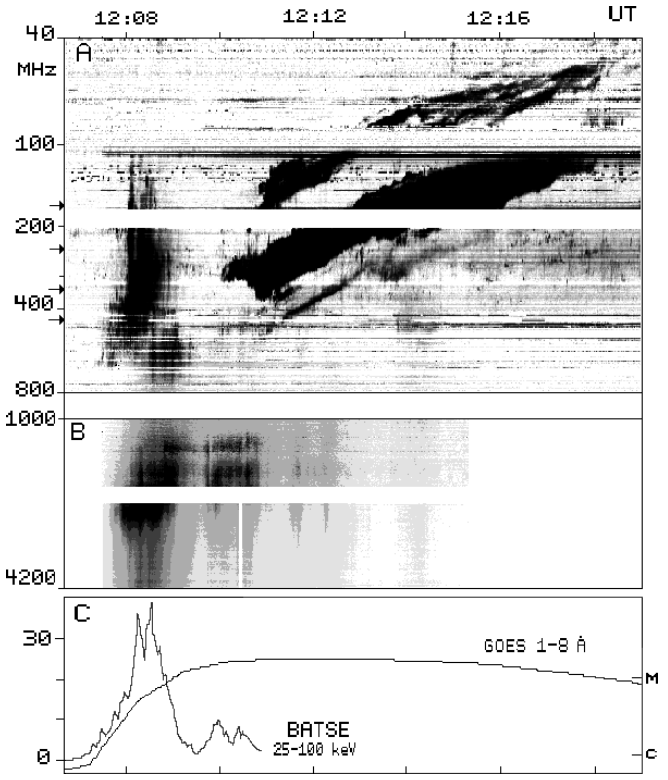

Fig. 3a–c. Event on 27 September 1993. The 40–4200 MHz dynamic spectrum (Tremsdorf **a** and Ondrejov **c**, courtesy M. Karlický), **C** GOES soft X-ray 1–8 Å (right axis) and CGRO BATSE 25–100 keV (left axis), $10^3\ counts\ (s\ 2000\ cm^2)^{-1}$, X-ray fluxes.

2.2.3. 27 December 1993

The radio spectrum of the type II burst (Fig. 5) shows both fundamental and harmonic lanes. Each lane is split into two bands, but only the high frequency split band is visible as a well-developed type II lane. The type II emission is preceded by a group of faint drift bursts with superposed continuum emission (9:12:56–9:13:27 UT, 250–600 MHz; the gap around 500 MHz is due to the subtraction of saturated signals from terrestrial transmitters).

Both high and low frequency cut–offs are well defined. They display a gradual or stepwise shift to lower frequencies. The group is associated with hard X-ray bursts. The decimetric emission lies in the vicinity of the backward-extrapolated harmonic type II lane, and is a similar *type II precursor* as in the previous events.

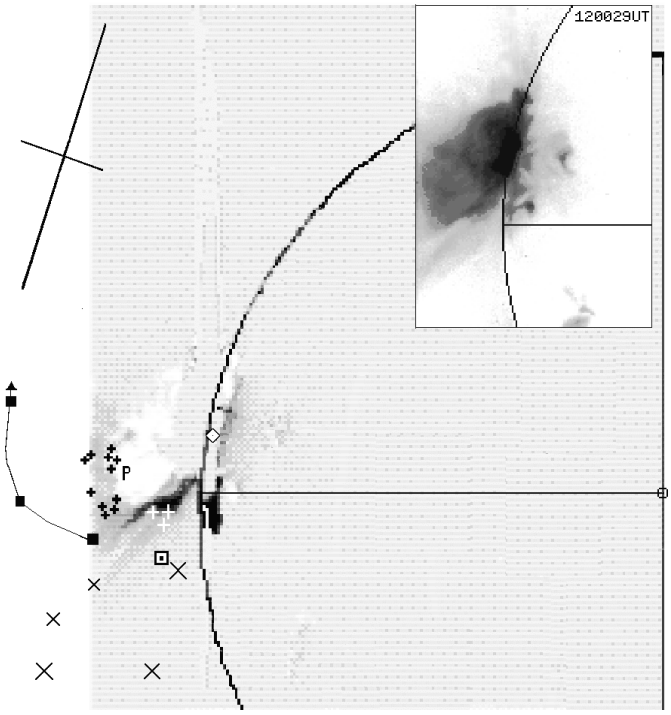

Fig. 4. Event on 27 September 1993. Superposition of the radio source centroids onto the difference between the *Yohkoh* SXT images after (12:37:17 UT) and before (12:00:29 UT) the flare (AlMg – filter, exposure 5.338 s). These are the only available full frame images for this event. No correction has been applied for the effect of solar rotation This explains the faint bright stripe on the inner side of the east limb which is drawn as a dark circle. Insert: *Yohkoh* SXT image at 12:00:29 UT. *Positions:* ♦ – Hα flare, + black and white – the impulsive phase type J and III bursts at 236, 327, 410 and 435 MHz, × – at 164 MHz, P – pulsations (*type II precursor*), ⊡ – 'arc', ■ – type II harmonics source ($2f_p$ and $3f_p$), big cross – the average half width of type II sources at 164 MHz.

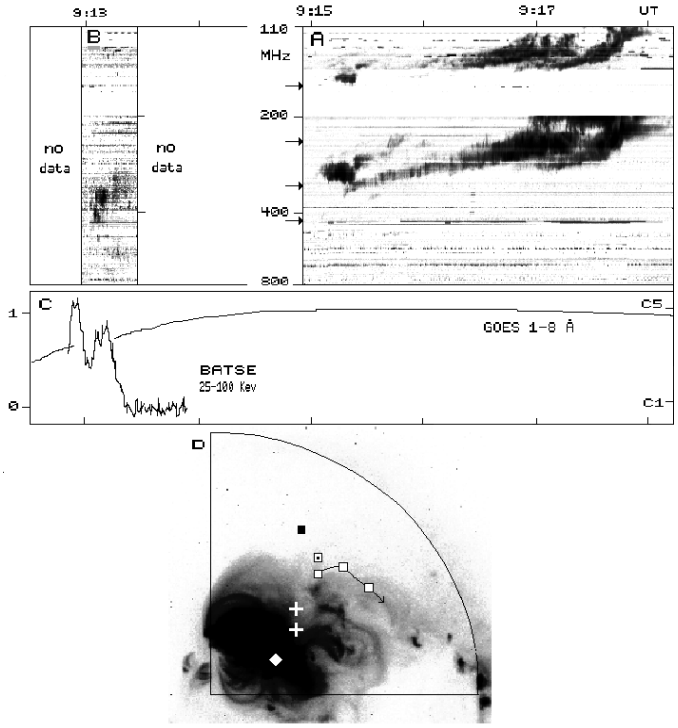

Fig. 5a–d. Event on 27 December 1993. Dynamic spectra of the type II – **A** and the *type II precursor* – **b** bursts, **c** – GOES and CGRO BATSE X-ray fluxes, **d** – positions of radio sources superposed upon *Yohkoh* SXT image (04:57 UT): ◊ – Hα flare, + *type II precursor* sources at 327 and 410 MHz, ⊡ – 'arc', □ – trajectory of the type II harmonic source at 327 and 236 MHz (upper split band), ■ – harmonic source at 236 MHz (lower split band).

The event displays a very clear *arc* in the fundamental and the harmonic mode (9:15:00–9:15:23 UT). It lies within the frequency gap between the split bands of the subsequent type II burst. The *arc* occurs while the soft X-ray flux is in its maximum phase.

The absolute heliographic positions of this event are uncertain because the low solar elevation makes them sensitive to ionospheric refraction. Nevertheless, the relative source positions are more reliable, since the event duration is much shorter than typical periods of ionospheric gravity waves. The source configuration is similar to the 27 September 1993 event: *precursor* bursts are located near the legs of a coronal loop system, while the *arc* and type II emission arise at greater altitude. The successive type II positions at ever lower frequencies are non-radially aligned above the loop system. The harmonic *arc* source at 327 MHz is not only spectrally, but also spatially located between the split bands of the harmonic type II lane. This strengthens the case for a physical relation between the *arc* and the subsequent type II burst.

2.2.4. 28 December 1993

The spectrum of this type II burst with its three harmonically related lanes (Fig. 6a) is similar to the one of 27 September 1993 (cf. Zlotnik et al. 1998).

Prior to the type II a group of faint fast drift bursts occurs (12:08:00–12:09:40 UT) whose spectrum is restricted to a rather narrow band (280–630 MHz), with global frequency drift of the brightest emission features at a normalized rate of about $-3{\cdot}10^{-3}$ s^{-1}. The backward extrapolation of the split bands of the harmonic type II lane leads to the vicinity of the high frequency cut-off (upper split band) and the body of the fast drift burst group (lower split band), respectively. Like the other events, this *precursor* is associated in time with energy release traced here by the temporal derivative of the soft X-ray burst. The event is the only case of our sample without an *arc* pattern.

The heliographic data (Fig. 6c) reveal three radially aligned type II burst sources north of the Hα flare position (diamond). The two white squares denote simultaneously appearing strong sources which are coincident at 236 and 164 MHz. A fainter type II source (black square) is only visible at 164 MHz. During the most intense type II emission the central source dominates at both frequencies. All heliographically detected type II burst sources belong to the second and later possibly to the third harmonic emission lane. The two burst sources are the successive

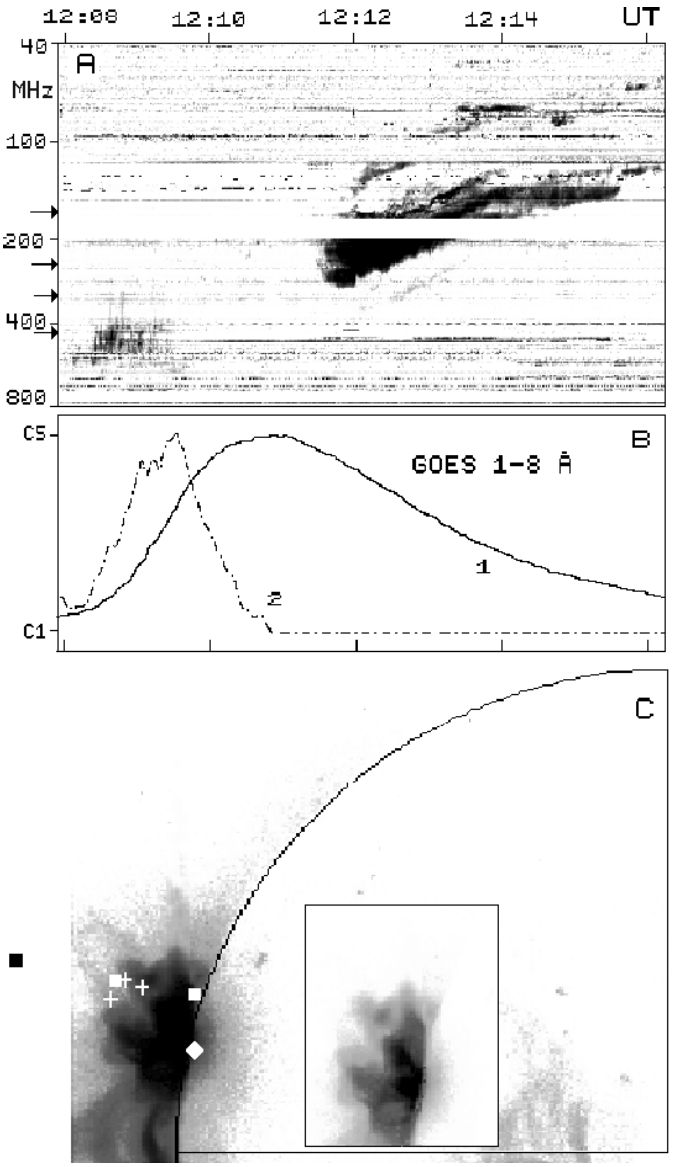

Fig. 6a–c. Event on 28 December 1993. **a** dynamic spectrum of the type II burst, **b** GOES soft X-ray flux 1–8 Å (1) and its derivative (2), **c** positions of radio sources superposed upon the *Yohkoh* SXT image (10:15 UT): ◊ – Hα flare, + presents a trajectory of an individual drift burst out the *type II precursor* at three frequencies 435, 410 and 327 MHz. There are three type II sources at 164 MHz (■ and two □) and two at 236 MHz (□). The main source lies near to the *type II precursor* source. Insert presents the same *Yohkoh* SXT image without the superposed source centroids.

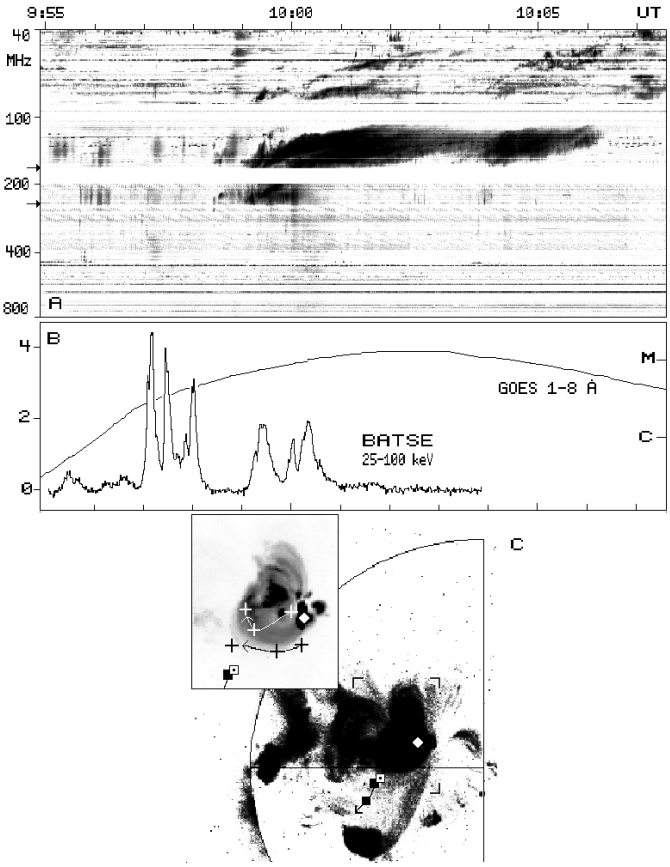

Fig. 7a–c. Event on 7 July 1994. **a** the 40–800 MHz dynamic spectrum, **b** GOES and CGRO BATSE X-ray fluxes, **c** burst positions superposed upon the *Yohkoh* SXT image (08:52 UT). ◊ – Hα flare. The insert presents the positions (trajectory) of two individual drift bursts out of the *type II precursor* at three frequencies. Black + – the burst at 09:55:43 UT at 327, 236 and 164 MHz, white + – the burst at 09:55:56 UT at 236 and 164 MHz (ascending branch) and 164 MHz (descending branch). ⊡ – 'arc', ■ – the first stage type II burst position (at 09:59 UT). The arrow to the south depicts later type II positions at the same frequency. The second stage type II (at 10:04 UT) occurs at the same position.

emission sites of the two split bands (see Aurass, Klein and Mann 1994). The strongest sources of type II emission display no significant outward motion at fixed frequency. Furthermore their projected position on the bright, i.e. dense, soft X-ray structures implies that the sources lie in front of the active region, since otherwise their intensity would be heavily reduced by free-free absorption. Hence the radio illuminated part of the shock front propagates along the line of sight toward the observer, i.e. along a strongly non-radial density gradient. The *precursor* burst sources, as shown in Fig. 6c) by the positions at three frequencies of one representative burst of the group, align along bright active region structures in the *Yohkoh* SXT image. Here, the *precursor* source sites are not located underneath the type II sources, presumably because of a projection effect caused by the type II exciter's movement towards the observer.

2.2.5. 7 July 1994

The event (Fig. 7a) consists of two successive type II bursts starting, respectively, at 09:58:30 (fundamental mode at about 90 MHz) and 10:03:20 UT (fundamental mode at about 80 MHz). The hard X-ray event (Fig. 7b) is a sequence of three groups of peaks($\sim$ 09:55–09:57 UT, $\sim$ 09:57–09:58:20 UT and 09:59–10:01 UT).

At radio wavelengths the first type II burst is preceded by fast drift bursts with a sharp cut-off at low frequencies ($\sim$130 MHz).

The high frequency cut-off is somewhere within the range (170–200) MHz (09:55–09:55:40 UT) and later evolves to about 450 MHz (∼09:57:10 UT). We can not analyze the detailed evolution of this shift since the subtraction of terrestrial transmitters creates an artificial spectral gap in the range $\sim$ (250–320) MHz. Simultaneously, a few short decimetric bursts also cluster around the backward extrapolated type II trace, but they are poorly described due to the subtraction of terrestrial transmitters. The high and low frequency cut-off of the decimetric/metric group of fast drift bursts and possibly the bursts in the vicinity of the extrapolated type II lane are signatures of a *type II precursor* which are similar to, though less conspicuous than the *precursors* during the other events.

The *arc* is not prominent in Fig. 7a, but appears clearly prior to the type II lane in the enlarged spectrum at the bottom of Fig. 9. It is accompanied at low frequencies by a type III burst, which is the first feature during this event that extends to the low frequency limit of the spectrograph. The hard X-ray counts are at the background level during the *arc*. The positions of two typical fast drift bursts are drawn on to the enlarged insert of the *Yohkoh* SXT image (Fig. 7c). The type J burst at 09:55:56 UT (white plus signs) traces a closed field structure revealed also by a coronal soft X–ray loop. The ascending source site at 236 MHz is close to the site of Hα emission. The central and eastern source sites are the ascending and descending J burst branch at 164 MHz. Another burst is observed at 327, 236 and 164 MHz (09:55:43 UT; black plus signs; decreasing frequency with increasing distance from the Hα flare site), tracing the boundary of an X-ray loop.

The heliographic data (Fig. 7c) confirm two different type II burst sources. The first leaves the active region to the south, as indicated by the alignment of sources at 237 and 164 MHz (second harmonic mode emission can be traced at 236 and 164 MHz in both split bands, *arc* emission at 236 MHz, only). The second type II burst at 10:03:20 UT is only faintly visible at 164 MHz (also in the second harmonic mode, *arc* emission followed by the lower split band). It starts at about the same site as the first type II burst. In Fig. 7, we have plotted the main source of the spectral features for simplicity, only. The type II source site is situated near the summit of precursor burst traces. The *arc* sources are close to the type II sources.

Fig. 8 compares the radio source locations with coronal magnetic field lines computed through a potential field extrapolation (Seehafer 1978 for the applied method). For this we used longitudinal field magnetograms (observed between 13:46 and 14:42 UT, Kitt Peak National Observatory). Fig. 8 gives an extrapolated field line map of AR 7746 and its surroundings (720 x 800 arcsec, north is up, west is right), with superposed field lines which turn or leave the extrapolation box in the height range $(5\text{–}10)\cdot 10^4$ km above the photosphere (top) and above $2\cdot 10^5$ km (bottom), respectively. The type J burst sources marked by white plus–signs in Fig. 7 align along a closed field structure.

The sources of the 09:55:43 UT burst are aligned along a bundle of field lines that are draped at low heights around the underlying closed magnetic structure and leave the extrapolation box above 200 000 km (Fig. 8, bottom). Both field line systems

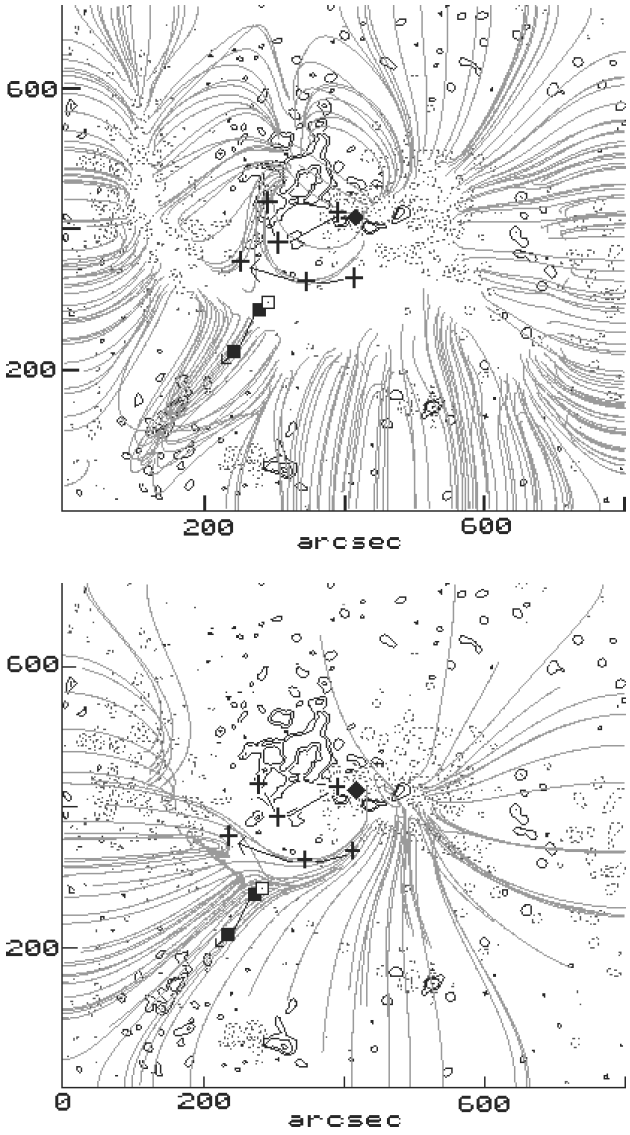

Fig. 8. Event on 7 July 1994. Positions of bursts as shown in Fig. 7 superposed upon the extrapolated magnetic field line map of AR 7746 (720×800 arcsec, north is up, west is right). Top–the field lines turning (or leaving the box sidewards) in the height range 50 000–100 000 km. Bottom–open field lines leaving the extrapolation box above 200 000 km.

are close to each other in the low atmosphere, and are rooted near the nominal site of the Hα flare (black diamond in Fig. 8). As inferred from the soft X-ray picture, the sources of the *arc* and the type II emission project to above the summit of the closed magnetic structures hosting the type J burst, i.e. on the region where open or large-scale interconnecting field lines leave the extrapolation box south-eastward in the bottom panel of Fig. 8.

2.3. Summary of observational results

The study of five type II bursts combining spectrographic and imaging data has revealed the following general features:

1. Type II radio sources lie above the summit of active region structures observed in soft X-rays, generally prefering inclined loops in the outskirts of an active region.
2. As usual, type II emission occurs after the impulsive flare phase, as identified by a hard X-ray burst (or the derivative of the soft X-ray burst) and meter wave bursts consisting of different kinds of fast drift bursts and continuum patches. However, only in one case of our study are the dm/m-wave fast drift bursts mainly of type III which extend down to the low frequency limit of the spectrograph (40 MHz). In the four other cases most (if not all) bursts exhibit a low frequency turnover or cut–off.
3. Two newly identified spectral features are described:
   (a) All five events display peculiar spectral features in their pre-type II burst emission which appear to be related to the type II exciter itself. In 4/5 cases the impulsive radio emission consists of a sequence of narrow-band bursts near the frequency of the backward extrapolated type II lanes. The high frequency envelope drifts at a normalized rate similar to the subsequent type II burst. In the fifth event the impulsive emission extends to the low frequency limit of the spectrograph, but its high frequency cut-off is again in the region to which the type II lane extrapolates. In projection on the solar disk the radio sources are located between the sites of the Hα flare and the type II source, in the legs of coronal loops revealed by the *Yohkoh* SXT or the radio images. The spectral range of the frequency gaps and cut-offs and the spectral and spatial location of the narrow-band bursts suggest that we have identified *precursors* that are physically related to the type II burst exciter. The *precursor* bursts are accompanied by hard X-ray emission.
   (b) In 4/5 events the type II emission is immediately preceded by a cluster of narrow-band fast drift bursts. The envelope of this spectral feature has an inverted U–shape, and is referred to as *arc*. The global bandwidth is comparable to an individual type II split band. The spectral morphology of the *arc* bursts resembles the herringbone fine structure elements of type II bursts. The *arc* has a similar fundamental-harmonic structure as the type II, but shows no recognizable band split. The enlarged spectra (Fig. 9) underline that the *arc* ends between the split bands of the type II burst. In 3/4 cases imaging observations show the *arc* source to have a distinctly different position from the subsequent type II lane. A common picture seems to be an *arc* source near the summit of active region loops, in between the sources of *precursor* and type II emission. However, the analyzed sample is too limited to exclude projection effects. In 2/4 cases the arc is accompanied on its low frequency side by a type III burst. In 3/4 cases there is no associated hard X-ray event (or positive derivative of the soft X-ray flux). The *arc* appears as a feature of type II bursts starting at rather high frequencies: 10 of 30 bursts studied at AI Potsdam between September 1993 and September 1997 display the *arc*. Nine of these ten events have their fundamental mode frequencies above 100 MHz.

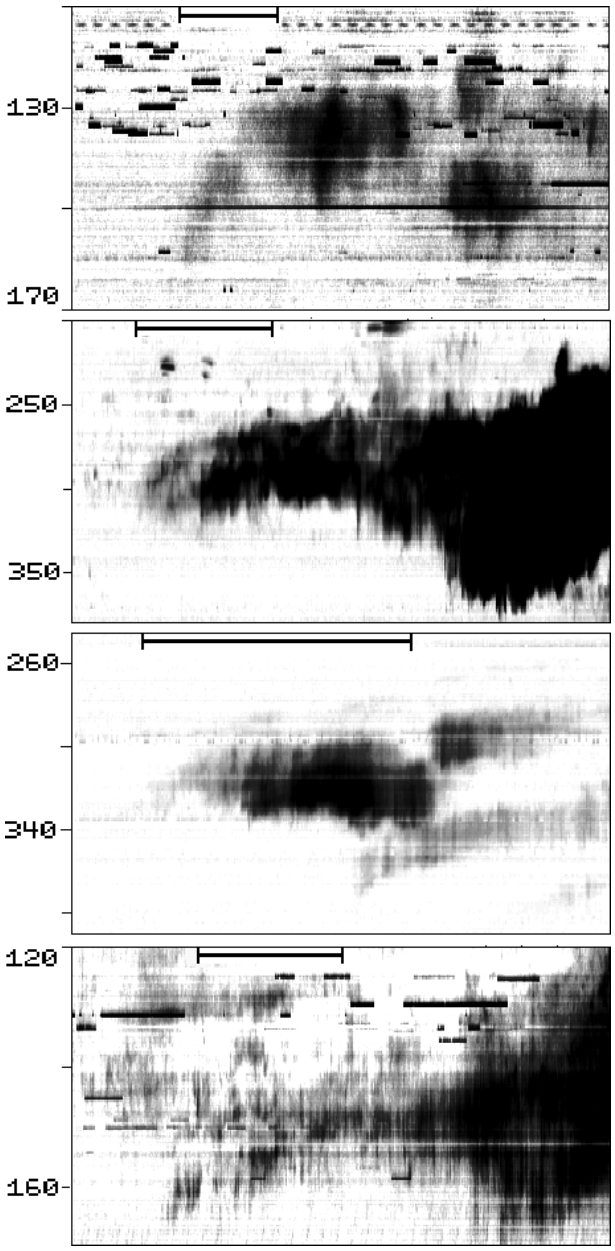

Fig. 9. Examples of *'arc'* feature. From top to bottom: 13 July 1994, 27 September 1993, 27 December 1993 and 7 July 1994. The horizontal bar marks a 20 s time scale.

3. Discussion

3.1. Type II source location

The localization of type II bursts confirms earlier results obtained with the *Culgoora Radioheliograph* and the NRH:

1. Type II emission starts above active region loops seen in soft X-rays (cf. Stewart 1977). The two different split band sources observed at the same frequency can be formed at

Table 1. Summary of radio and X-ray observations

Parameter/Date	27 September 1993	27 December 1993	28 December 1993	7 July 1994	13 July 1994
NOAA location	7590 (N11E80)	7640 (N07W13)	7645 (N12E83)	7746 (N13E18)	7746 (N10E66)
SXR(GOES,UT)	12:04/12:12/12:18 –/M1.8	09:12/09:15/09:41 SF/C4.8	12:05/12:10/12:14 –/C4.6	09:53/10:00/10:23 1N/M1.3	11:42/11:44/11:56 SF/B3.2
HXR (BATSE) counts	12:06.7/12:08.6/12:11 ≥ 38500	9:12.7E/9:12.9/9:14 1160	12:08/12:08.9/12:09U ≥ 5100	9:55/9:57/10:03 ≥ 4389	no observation
Precursor					
impulsive dm-m	12:07.3–12:09.5	09:12.9E-09:13.5U	12:08.1–12:09.7	09:53.6–09:58	11:39.5–11:44.3
range, MHz	700–80	600–250	$\geq 630 - 280$	550–110	$350 - \leq 40$
cm-burst, sfu	310 & 56	23	130 & 25	23 & 17	no data
D_f,MHz s^{-1}	−3–4	too short	−1.55	−2	0.5–1
D_f/f	5.5–7.4 10^{-3}	too short	2.8 10^{-3}	6.8 10^{-3}	2.2–3.8 10^{-3}
'Arc'	yes	yes	no	yes (yes)	yes
Type II:					
start/end, UT	12:10.0–12:19.0U	09:15–09:18	12:11.4–12:18.5	09:58.4–10:06D	11:45.3–11:49D
start, MHz:					
Fundamental f_p	≈ 180	≈ 180	146	124(≥ 85)	
Harmonic $2f_p$	377	360	303	250(≥ 170)	≈ 170
Third $3f_p$	547		≥ 410		
Ratio (averaged) $f_p/2f_p/3f_p$	1:2.06:2.83	1:2.01	1:2.09:2.97	1:1.96 (1:2.03)	–
Drift, MHz s^{-1}:					
f_p	−0.48	−0.38	−0.46	−0.20 (−0.22)	–
$2f_p$	−1.0	−0.80	−0.98	−0.39 (−0.46)	−0.33
$3f_p$	−1.57	–	−1.50		
D_f/f	$4 \cdot 10^{-3}$	$2.7 \cdot 10^{-3}$	$4 \cdot 10^{-3}$	$3 \cdot 10^{-3}$	$2.6 \cdot 10^{-3}$
Lane split	yes	yes	yes	yes (yes)	yes
Herring. struct.	yes	yes	yes	yes (yes)	yes
Source struct.: f_p	m.s.+ s.s	m.s.	–	–	–
$2f_p$	m.s.+ s.s	m.s.	m.s.+ two s.s.	m.s. (m.s.)	m.s.
$3f_p$	m.s.		m.s.		

f_p, $2f_p$ and $3f_p$ refer to the fundamental, harmonic and third harmonic, respectively. M.s. – main source, s.s. – secondary source, cm-burst – flux density at 3 and 9 GHz, 1 sfu (solar flux units) = $10^{-22} Wm^{-2} Hz^{-1}$. E – earlier, U – uncertain, D – after. In brackets, we give values for the second type II on July 7, 1994.

different sites above the active region (cf. Aurass, Klein and Mann 1994).

2. Type II sources are the farther away from the active region, the lower the observed frequency. The alignment of sources at successively lower frequencies is often not radial. The low frequency sources rather seem to bend away from the active region (cf. Nelson and Robinson 1975; Aurass, Hofmann and Urbarz 1998).

These observations are in agreement with the idea that type II emission does not outline the entire shock front, but occurs where the shock wave intersects pre-existing structures (e.g. Stewart 1984), or, alternatively, that it is driven by a piston with smaller scale than a CME, e.g. a jet. When compared with *Yohkoh* soft X-ray images, the events bear ambiguous evidence on the driver of the coronal shock wave: while we could identify in one case structural changes of coronal loops underneath the site where the type II burst started, in line with the result of Gopalswamy et al. (1997), the soft X-ray loops remained unchanged in another case. This may signify that either the driver gas has low temperature, such as a surge, or that the compression of the ambient plasma by the shock wave is too low to be detectable, i.e. a shock with low Mach number.

3.2. Type II precursor features

The *precursor* phenomenon is visible in various types of bursts (type III of negative and positive slope, due to electron beams propagating along and against the local density gradient, J, U, pulsations) through their well defined cut-offs at high and low frequencies, and a gradual drift of the high frequency cut-off towards lower frequencies. It is remarkable that different kinds of bursts display a similar gradual drift of their starting frequency, sometimes also of the low frequency cut-off. The normalized drift rate is comparable with that of the following type II lanes

(Table 1). The spectral behaviour and the location of the bursts in active region structures between the site of Hα emission and the subsequent type II source suggest that the *precursor* phenomena are tracers of a propagating disturbance before it becomes the exciter of type II emission. From the frequency drift the disturbance must be a MHD wave or plasma propelled in the ambient corona. The earliest detection of the cut-offs and the location of the radio burst sources show that the disturbance can be traced back to the time between start and maximum of flare energy release revealed by hard X-ray emission and in low coronal structures of the flaring active region. The present study hence reaches a similar conclusion on the launch time as Vršnak et al. (1995), but since the *precursor* phenomena directly trace the early history of the type II exciter, the conclusion requires no hypothesis on the coronal propagation of the type II exciter.

The *precursor* becomes visible by peculiar features in the impulsive radio bursts prior to the type II emission. While the bursts themselves are indicators of electron beam acceleration, there is no possibility to decide from the available data whether the beams are accelerated by the disturbance which later gives rise to the type II emission, or whether the basic effect of the disturbance is to suppress a part of the burst spectrum.

3.3. The arc

Judging from its spectral and spatial appearance (between split bands of the type II emission, herringbone-like elementary pattern) the *arc* is closely related to the onset of the radio emission from electrons accelerated in the type II shock wave. Some specific spectral characteristics (inverted U envelope, almost no band split) imply, however, a basic difference with the type II emitting process. Since the *arc* source is located near the summit of coronal loops, close to, but different from the type II source, it is tempting to relate the *arc* with the change of propagation conditions of the disturbance at the transition from closed to open magnetic fields. The appearance of type III bursts on the low frequency side of the harmonic *arc* during two events supports this idea. This scenario also explains the statistical finding from the AI Potsdam spectral studies that the *arc* is a specific feature of type II bursts with high (≥ 100 MHz at the fundamental mode) starting frequency. It agrees furthermore with the expectation that a small-amplitude MHD disturbance will steepen into a shock wave in regions of small Alfvén speed, e.g. in the regions of weak magnetic field near the summits of coronal loops (cf. also Uchida 1974, Aurass, Hofmann and Urbarz 1998). In this scenario we ascribe the U-shaped envelope of the *arc* to the recently formed shock wave propagating across the summit of a loop before being refracted out of it into the overlying open field structure.

Acknowledgements. We are grateful to the staff of Potsdam-Tremsdorf and Nançay Radio Observatories. NSO / Kitt Peak data used here are produced cooperatively by NSF/NOAO, NASA/GSFC and NOAA/SEL. The authors are thankful for access to *Yohkoh* data at Mullard Space Center (UK) and at ISAS Tokyo (Japan), to BATSE/CGRO and GOES data at the Solar Data Analysis Center at NASA/GSFC. H.A. profited from his participation at the CDAW3–Workshop 1998. The Nançay Radio Observatory is funded by the French Ministry of Education, the CNRS and the Région Centre. The research of A. K. is supported by the Deutsche Forschungsgemeinschaft under Grant No. DFG/Au 106/6-2.

References

Aurass H., 1992, Ann. Geophysicae 10, 359–366
Aurass H., 1997, In: Trottet G. (ed.), Lecture Notes in Physics 483, 135
Aurass H., Hofmann A., Urbarz H.-W., 1998, A&A 334, 289
Aurass H., Klein K.-L., Mann G., 1994, ESA SP-373, 95
Aurass H., Magun A., Mann G., 1994, Space Sci. Rev. 68, 211
Bougeret J-L., 1985, In: Tsurutani B.T., Stone R.G. (eds.) Collisionless Shocks in the Heliosphere. Reviews of Current Reseach. AGU GN-34, Washington DC, 13
Dennis B.R., Zarro D.M., 1993, Solar Phys. 146, 177
Gopalswamy N., Kundu M.R., 1992, In: Zank G.P., Gaisser T.K. (eds.) Particle Acceleration in Cosmic Plasmas. American Institute of Physics, New York, p. 257
Gopalswamy N., Kaiser M.R., Lepping R.P., et al., 1998, J. Geophys. Res. 103, 307
Gopalswamy N., Kundu M.R., Manoharan P.K., et al., 1997, ApJ 486, 1036
Hildner E., Bassi J., Bougeret J.L., et al.,1986, In: Kundu M.R., Woodgate B.E. (eds.) Energetic Phenomena on the Sun. NASA CP-2439
Karlický M., Jiřička K., 1996, Solar Phys. 1996, v.163, 171–181
Mann G., 1995, In: Benz A.O., Krueger A. (eds.) Lecture Notes in Physics 444, 183
Mann G., Aurass H., Voigt W., Paschke J., 1992, ESA SP-348, 129
Mann G., Classen T., 1995, A&A 304, 576
Mann G., Classen T., Aurass H., 1995, A&A 295, 775
Nelson G.J., Melrose D.R., 1985, In: McLean D.J., Labrum N.R. (eds.) Solar Radiophysics. Cambridge Univ. Press, Cambridge, UK, p. 333
Nelson G.J., Robinson R.D., 1975, PASA 2, 370
Seehafer N., 1978, Solar Phys. 58, 215
Stewart R.T., 1977, PASA 3, 157
Stewart R.T., 1984, Solar Phys. 94, 379
The Radioheliograph Group, 1989, Solar Phys. 120, 193
Tsuneta S., Acton L., Bruner M., et al., 1991, Solar Phys. 136, 37
Uchida Y., 1974, Solar Phys. 39, 431
Vršnak B., Ruždjak, Zlobec P., Aurass H., 1995, Solar Phys. 158, 331
Zlotnik E.Ya., Klassen A., Klein K.-L., Aurass H., Mann G., 1998, A&A 331, 1087